Journal of Chemical Health Risks

www.jchr.org

JCHR (2025) 15(6), 3292-3301 | ISSN:2251-6727

Synthesis and Performance Assessment of Calcium- and Magnesium-Coated Activated Alumina Granules for Sustainable Fluoride Removal from Groundwater

Kamlakar Y. Nikhade, Hitesh K. Dewangan

Department of Chemistry, Shri Rawatpura Sarkar University, Raipur-492015, Chhattisgarh, India

(Received: 25 October 2025 Revised: 27 November 2025 Accepted: 16 December 2025)

KEYWORDS

Activated Alumina, Fluoride Removal, Defluoridation, Groundwater Remediation, Sol-Gel Synthesis, Adsorption Isotherms

ABSTRACT:

Groundwater contamination by fluoride ions poses significant public health risks, necessitating efficient remediation strategies. This study presents the synthesis and evaluation of calcium (Ca) and magnesium (Mg)-coated activated alumina (Ca-Mg-AA) granules as a multifunctional adsorbent for defluoridation. Activated alumina granules were prepared via a modified sol-gel method, followed by sequential dip-coating with Ca and Mg precursors and sintering at 600 °C. The modified adsorbents were characterized using XRD, SEM, TEM, FTIR, and TG-DTA, confirming the formation of nanocrystalline γ-Al_2O_3 with uniform CaO and MgO coatings (40-70 nm particles), enhanced surface porosity, and thermal stability up to 1000 °C. Batch adsorption experiments assessed the effects of pH (3-7), adsorbent dose (10-50 mg), and contact time (0-120 min) on fluoride removal from synthetic solutions (1-10 mg/L). Optimal performance was achieved at pH 5, 30 mg dose, and 60 min contact time, with Ca-Mg-AA exhibiting superior removal efficiency (up to 85%) compared to pure AA (82%) and Ca-AA (75%), attributed to synergistic ion exchange and surface complexation. Equilibrium data followed the Freundlich isotherm, indicating heterogeneous multilayer adsorption. The coatings extended the effective pH range and minimized byproduct toxicity, highlighting Ca-Mg-AA as a sustainable, low-cost solution for fluoride-affected regions, with potential for simultaneous heavy metal removal.

1. Introduction

Groundwater serves as a primary source of drinking water for billions of people, yet its quality is increasingly compromised by both natural and anthropogenic contaminants, posing serious public health challenges. [1] Among these pollutants, fluoride is one of the most prevalent, affecting over 200 million people across more than 100 countries. [2] When fluoride concentrations exceed the World Health Organization (WHO) guideline of 1.5 mg/L, prolonged exposure can lead to dental and skeletal fluorosis, as well as damage to vital organs such as the liver, kidneys, thyroid, and brain. [3] Compounding the issue, fluoride-contaminated aquifers often contain toxic heavy metals such as arsenic, chromium, lead, and mercury. Arsenic exposure is associated with skin disorders and carcinogenic effects, chromium can induce organ toxicity, lead disrupts neurological development, and mercury damages the nervous system.[4] Therefore, developing efficient and reliable remediation methods is essential to ensure safe drinking water.

Activated alumina (AA) is one of the most widely used materials for fluoride adsorption owing to its high surface area, affordability, and strong interaction with fluoride ions via ion exchange and surface complexation.[5] However, its performance is restricted by its narrow operational pH range, functioning effectively only under mildly acidic conditions (pH 5-6). [6] Furthermore, regeneration of spent AA typically requires harsh chemicals, leading to the formation of toxic aluminum fluoride complexes that pose environmental hazards.

To address these limitations, recent research has focused on modifying activated alumina with alkaline earth metals such as calcium (Ca) and magnesium (Mg). [7] Such surface coatings enhance adsorption capacity, expand the effective pH range, and minimize harmful byproduct generation during regeneration. Additionally,

Journal of Chemical Health Risks
www.jchr.org
JCHR (2025) 15(6), 3292-3301 | ISSN:2251-6727

these modified adsorbents demonstrate improved efficiency for co-removal of other contaminants like arsenic and chromium through synergistic mechanisms such as ion exchange and co-precipitation.[8-9]

The present study is centered on the synthesis of Ca- and Mg-coated activated alumina granules for efficient defluoridation of groundwater. The work further investigates the impact of these coatings on adsorption performance and assesses their ability to remove fluoride from contaminated water. This strategy aims to develop a sustainable, low-cost, and multifunctional adsorbent suitable for water treatment in fluoride-affected regions.

2. Experimental Methodology

2.1 Synthesis of Activated Alumina Granules

Activated alumina granules were synthesized using a modified sol–gel method. Initially, aluminum sulfate was dissolved in double-distilled water to obtain a transparent solution. A 0.1 M sodium hydroxide solution was added dropwise under constant stirring until precipitation was achieved at approximately neutral pH. The suspension was then maintained in a water bath at 70 °C for 6–7 hours to facilitate gelation, followed by overnight settling. After settling, the supernatant was decanted, and the solid mass was filtered and repeatedly washed with warm distilled water to ensure complete removal of sulfate residues.

To aid peptization, a few drops of concentrated nitric acid were added to the washed precipitate, which was subsequently ultrasonicated to obtain a uniform sol. This sol was dispensed using a dropper into a paraffin oil–ammonia bath, resulting in the formation of spherical beads of approximately 3 mm in diameter. The formed granules were dried in a hot air oven at 30-40 °C and then calcined at 600 °C for 3 hours to yield porous γ-alumina.

2.2 Surface Coating with Calcium and Magnesium

To improve adsorption performance, the activated alumina granules were sequentially coated with calcium and magnesium using a dip-coating approach as shown in table 1.[10]

Calcium coating: The alumina granules were first immersed in a calcium chloride solution (0.1–0.5 M, optimized through preliminary experiments) maintained at pH 9. After 1 hour of soaking, the granules were dried at 100 °C for 2 hours and subsequently sintered at 600 °C for 4 hours to develop a stable CaO layer on the surface.

Magnesium coating: The calcium-coated granules were then introduced into a magnesium chloride solution (0.1–0.5 M) adjusted to pH 12 and kept for 1 hour. Similar to the previous step, the treated granules were dried at 100 °C and sintered at 600 °C for 4 hours to obtain Ca–Mg-modified activated alumina (Ca-Mg-AA).

Table 1: List of samples prepared

Sr. No.	Samples	Code
1	Calcium coated activated alumina	Ca@AA
2	Magnesium coated activated alumina	Mg@AA
3	Calcium and magnesium coated activated alumina	Ca, Mg @AA

3. Characterisation Technique:

A series of analytical tools were employed to evaluate the structural, morphological, chemical, and thermal characteristics of the synthesized activated alumina and Ca–Mg-coated granules.

X-ray Diffraction (XRD):

Crystalline phases and structural changes after surface modification were identified using a *Rigaku XRD system* with Cu Kα radiation (λ = 1.5406 Å). Scans were recorded within a predefined 2θ range, and the obtained diffractograms were matched with standard JCPDS files for phase confirmation.[11]

Scanning Electron Microscopy (SEM):

The surface texture and coating behavior were visualized using a *JEOL scanning electron microscope*. Samples were sputtered with a thin layer of gold before analysis to prevent charging.[12]

Transmission Electron Microscopy (TEM):

Nanostructural insights, coating thickness, and crystallite orientation were assessed using a *JEOL TEM*. High-resolution imaging and SAED (selected area electron diffraction) patterns were used to validate the crystalline structure and interface characteristics.

Journal of Chemical Health Risks
www.jchr.org
JCHR (2025) 15(6), 3292-3301 | ISSN:2251-6727

Fourier Transform Infrared Spectroscopy (FTIR):

Chemical bonding and functional groups present on the adsorbent surface were examined using a *Bruker FTIR spectrometer* over the 400–4000 cm^{-1} range. Characteristic vibrations corresponding to Al–O, Ca–O, Mg–O, and –OH groups provided confirmation of surface modification.[13]

Thermogravimetric and Differential Thermal Analysis (TG-DTA):

The thermal decomposition behavior and phase transitions of the samples were monitored using a TG-DTA instrument under a controlled heating rate. Weight loss steps were correlated with dehydration, dehydroxylation, and coating layer stabilization events.

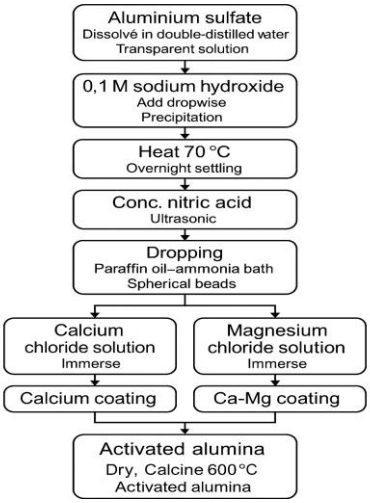

Figure 1: Flow chart of synthesis of Ca and Mg coated activated alumina by sol gel method

4. Results and Discussion:

The X-ray diffraction (XRD) pattern of the synthesized alumina adsorbent shown in figure 2 exhibits broad diffraction peaks characteristic of poorly crystalline γ-Al_2O_3. Prominent reflections are observed at approximately 31.2°, 37.5°, 45.8°, 60.7°, and 66.8° (2θ), which can be indexed to the (220), (311), (400), (511), and (440) planes of defect-spinel structured γ-Al_2O_3 (JCPDS No. 20-063).[14] The absence of sharp reflections corresponding to α-Al_2O_3 (corundum phase) confirms that the material has retained a highly disordered and nanocrystalline structure, which is desirable for adsorption applications. The broadening of peaks further suggests small crystallite size and high surface defect density, both of which contribute to enhanced fluoride uptake through surface complexation and ion exchange mechanisms.[15]

The presence of amorphous halos and peak broadening indicates a high surface area and porous structure, which facilitates rapid mass transfer and increased accessibility of active adsorption sites. Such structural features of γ-Al_2O_3 have been widely reported to improve its affinity toward fluoride ions.[16]

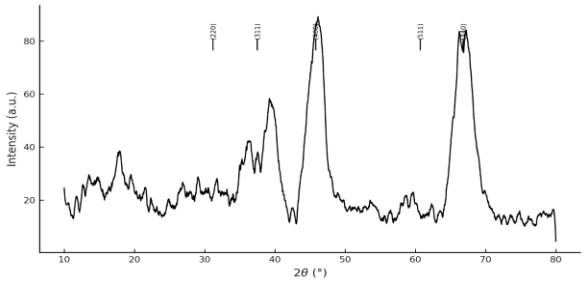

Figure 2: X-ray diffraction plot of pure activated alumina prepared via sol gel method

The FTIR spectra of bulk alumina display well-defined bands, signifying the development of a more ordered structural arrangement. As shown in Figure 3, two characteristic peaks appear around 557 cm^{-1} and 519 cm^{-1}. The band near 600 cm^{-1} exhibits slightly higher intensity, which, as reported by Ying et al., corresponds to an increased occupation of octahedral sites. [17] These sites possess higher coordination and tend to be populated under elevated thermal conditions. A similar trend was observed by Baraton and Quintard in alumina samples annealed at 950 °C for 5 h. [18] Furthermore, a noticeable narrowing of the alumina bulk band allows the identification of a shoulder around 1042 cm^{-1}, attributed to the Al–O stretching vibrations of surface species. The absorption feature near 2920 cm^{-1} confirms that a portion of physically adsorbed water remains after synthesis, while the band at 1324 cm^{-1} signifies the presence of residual nitrates. Overall, the infrared analysis suggests that alumina with sharp Al–O vibrational peaks can be effectively obtained when the ignition temperature exceeds 800 °C, which is in good agreement with the XRD findings discussed earlier.

Journal of Chemical Health Risks
www.jchr.org
JCHR (2025) 15(6), 3292-3301 | ISSN:2251-6727

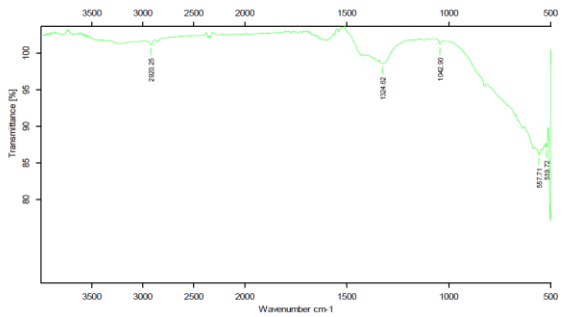

Figure 3: FT-IR spectra of pure activated alumina prepared via sol gel method

The surface morphology of the synthesized activated alumina granules was examined using Scanning Electron Microscopy (SEM), and the corresponding images are shown in Fig. 4(a–b). The SEM micrograph of the pure activated alumina, prepared through the hydrolysis route, displays a uniform distribution of thin, plate-like or flake-shaped structures, resembling leaf-like formations. Such morphology is typical of γ-Al_2O_3, indicating the presence of a highly porous structure favorable for adsorption applications.[19] After sintering at 600 °C, the morphology changes noticeably, as shown in Fig. 4. The particles become more compact and agglomerated, forming a continuous interconnected network due to particle fusion at higher temperatures. The formation of neck-like connections between grains confirms the onset of sintering and partial densification.[20] The estimated grain size is around 50 nm, which agrees well with the crystallite size calculated from XRD data using the Scherrer equation. Overall, SEM observations reveal that the activated alumina granules transform from a loosely packed flake-like structure to a more consolidated and agglomerated morphology after heat treatment, demonstrating enhanced grain connectivity and crystallinity with increasing temperature.

The morphology and particle size of the coated activated alumina granules were further examined using Transmission Electron Microscopy (TEM), as shown in Fig. 5(a–b). The TEM image of calcium-coated activated alumina [Fig. 5(a)] reveals the presence of uniformly distributed nanoparticles with quasi-spherical to irregular shapes. The particles are slightly aggregated, which is typical for nanosized oxides due to surface energy effects. The particle size is observed to be in the range of 40–70 nm, indicating the successful formation of nanoscale CaO layers on the alumina surface. The distinct contrast between lighter and darker regions suggests a dense coating layer of calcium on the porous alumina matrix.[21]

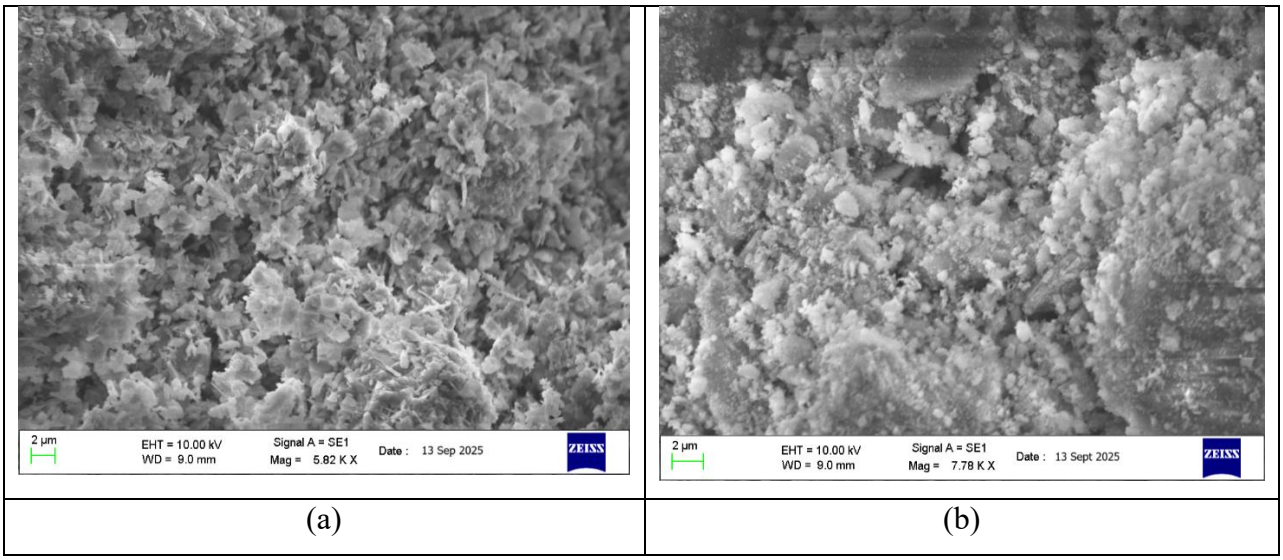

Figure 4: SEM micrographs of prepared activated alumina coated with (a) Ca and (b) Mg

Journal of Chemical Health Risks
www.jchr.org
JCHR (2025) 15(6), 3292-3301 | ISSN:2251-6727

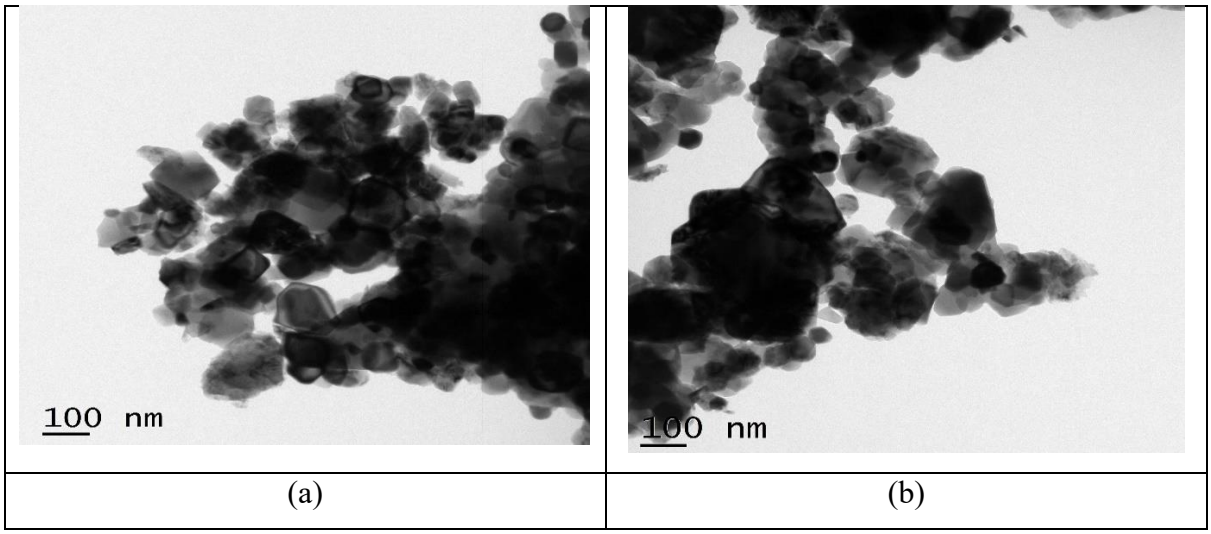

Figure 5: TEM image of prepared activated alumina coated with (a) Ca and (b) Mg

Similarly, the TEM micrograph of magnesium-coated activated alumina [Fig. 5(b)] shows a collection of well-dispersed, fine nanoparticles with an average size close to 50 nm. The particles appear interconnected and form small clusters, confirming the uniform deposition of MgO over the alumina framework. The relatively lighter contrast regions indicate a thin and homogeneous Mg layer, which supports the formation of a well-coated Ca–Mg-modified alumina structure.

Overall, TEM observations confirm that both calcium and magnesium coatings were successfully achieved, leading to fine, nanostructured, and uniformly distributed layers over the activated alumina granules. Such nanoscale coatings are expected to enhance the surface activity and adsorption efficiency of the material.

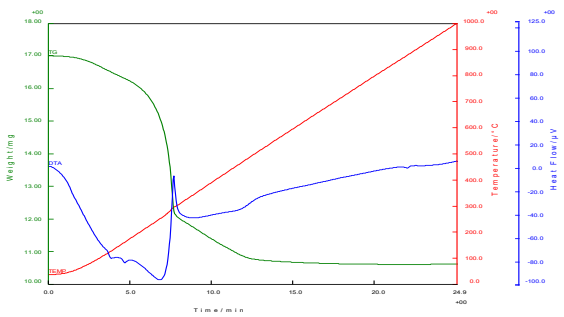

Figure 6: TG-DTA curve of pure activated alumina prepared via sol gel method

Thermal analysis was performed at a heating rate of 20 °C min^{-1} up to 1200 °C, and the resulting TG/DTA traces are presented in Figure 6. The mass-loss behaviour occurs in two main stages.[22] In the low-temperature region up to the endothermic feature near 250 °C, loss of physically and chemically bound water is dominant as γ-AlOOH converts toward γ-Al_2O_3, accompanied by volatilisation of loosely held species. Between ≈150 and 340 °C a substantial loss (~24.75%) is measured, exceeding the simple stoichiometric loss expected for boehmite dehydration; this extra loss is attributed to strongly adsorbed hydration water often found in ultrafine or pseudo-boehmite-like powders. Further gradual mass reduction at higher temperatures reflects removal of residual hydroxyl groups from the intermediate γ-alumina. A subsequent mass change between ~340 and 550 °C (≈11.556%) is associated with the development of a more crystalline alumina phase; beyond this step the TGA curve is essentially flat up to 1000 °C. The overall mass loss for the sample is ≈36.30%. The DTA trace shows exothermic features that correlate with these TG events; the exotherm around 420 °C is consistent with decomposition of residual nitrates (as supported by FT-IR), and the minimal weight change near 1000 °C indicates conversion to the thermodynamically stable α-Al_2O_3, in agreement with the XRD results.

Journal of Chemical Health Risks
www.jchr.org
JCHR (2025) 15(6), 3292-3301 | ISSN:2251-6727

5. Stock solution preparation and calibration of atomic absorption spectrophotometer:

A fluoride stock solution of 1000 mg/L concentration was prepared by accurately dissolving 2.21 g of sodium fluoride (NaF, analytical grade) in double-distilled water and making up the volume to 1 liter in a volumetric flask. Sodium fluoride was chosen as the fluoride source because it is highly soluble and provides a stable concentration of fluoride ions in aqueous medium. The prepared stock solution was stored in a tightly closed polyethylene bottle to prevent contamination and evaporation losses. From this stock, working fluoride solutions of desired concentrations (e.g., 1-10 mg/L) were prepared by appropriate serial dilution using double-distilled water immediately before each experiment. All glassware used in the preparation was thoroughly cleaned with dilute nitric acid followed by rinsing with distilled water to avoid any ionic interference during analysis.[23]

The atomic absorption spectrophotometer was calibrated using known concentration of this stock solution. The absorbance corresponding to concentration 1, 2, 3, 3, 4, 5 ppm was noted using AAS for fluoride ions. The absorbance values of the prepared fluoride standards were measured, and a calibration curve was constructed as shown in Figure 7. The corresponding calibration equation and correlation coefficient (R^2) are also presented in the figure 7.

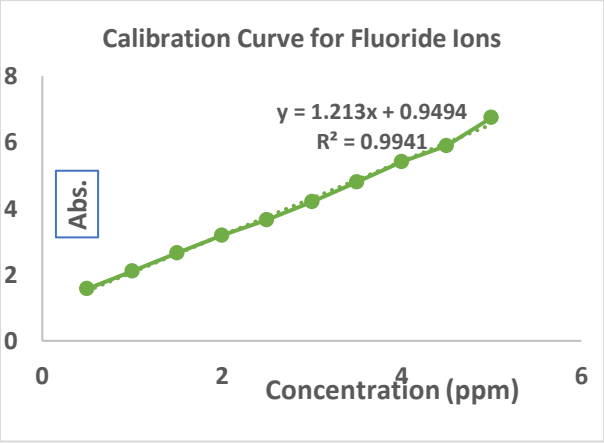

Figure 7: AAS Calibration curve for fluoride adsorption

Effect of pH on Fluoride Removal Efficiency:

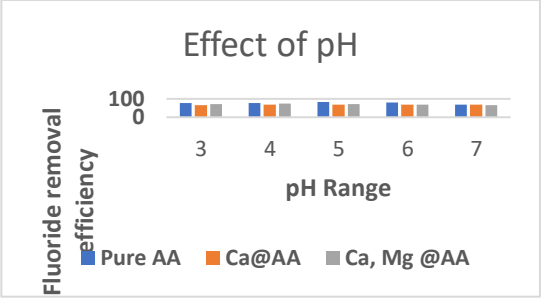

Figure 8: Effect of pH on Fluoride Removal Efficiency of pure AA, Ca@AA and Ca, Mg@AA

Figure 8 represents the variation in fluoride removal efficiency of pure activated alumina (AA), calcium-coated alumina (Ca@AA), and calcium–magnesium-modified alumina (Ca-Mg@AA) across different pH values ranging from 3 to 7. The data reveal that pH plays a crucial role in governing fluoride adsorption behavior.[24] All adsorbents exhibit maximum fluoride uptake under mildly acidic conditions, particularly around pH 5. At this pH, pure activated alumina demonstrates the highest removal efficiency (about 82%), while Ca@AA and Ca-Mg@AA achieve slightly lower but comparable efficiencies (approximately 70-75%). The enhanced performance in acidic media can be linked to the positively charged alumina surface, which promotes electrostatic attraction between surface hydroxyl groups and negatively charged fluoride ions.[25]

As the pH increases toward neutral values, a gradual decline in fluoride removal efficiency is observed for all samples. This decrease can be attributed to surface deprotonation, which reduces the positive charge density on the adsorbent surface, leading to electrostatic repulsion between fluoride ions and the adsorbent. Additionally, the possible formation of soluble fluoride–metal complexes at higher pH values may further hinder adsorption. Although the Ca and Mg-modified alumina samples show slightly lower fluoride uptake in acidic media compared to pure alumina, they retain a relatively stable adsorption efficiency over the entire pH range studied. This indicates that surface modification with alkaline earth metals enhances the structural and chemical stability of alumina, thereby extending its effective operational pH range and making

Journal of Chemical Health Risks
www.jchr.org
JCHR (2025) 15(6), 3292-3301 | ISSN:2251-6727

it more suitable for real water treatment systems with variable pH conditions.[26]

Effect of Adsorbent Dose on Fluoride Removal:

The graph illustrates the influence of adsorbent dosage on the fluoride adsorption capacity for pure activated alumina (AA), calcium-modified AA (Ca@AA), and calcium–magnesium-modified AA (Ca,Mg@AA). As shown, the adsorption capacity increases with adsorbent dose up to 30 mg, after which it tends to stabilize or slightly decrease. This behavior indicates that increasing the adsorbent dose provides more active surface sites for fluoride binding, enhancing removal efficiency initially. However, beyond the optimum dose, the adsorption capacity per unit mass decreases due to aggregation of particles and overlapping of adsorption sites, leading to a reduction in available surface area.

Among all samples, Ca,Mg@AA exhibits the highest fluoride removal efficiency across all dosages, followed by pure AA and Ca@AA. The enhanced performance of Ca,Mg@AA can be attributed to the combined effect of Ca and Mg ions, which enhance fluoride ion affinity and improve surface reactivity. Therefore, an adsorbent dose of around 30 mg can be considered optimal for achieving effective fluoride adsorption under the given experimental conditions.

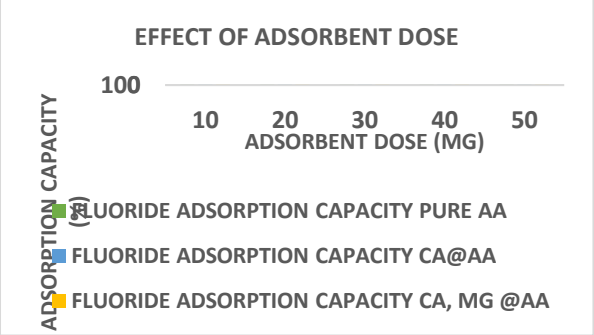

Figure 9: Effect of adsorbent dose on Fluoride Removal Efficiency of pure AA, Ca@AA and Ca, Mg@AA

Effect of Contact Time on fluoride Removal Efficiency:

Figure 10 illustrates the influence of contact time on the fluoride removal efficiency of pure activated alumina (AA), calcium-coated alumina (Ca@AA), and calcium–magnesium-modified alumina (Ca-Mg@AA). The experiments were conducted at various contact times to determine the equilibrium period for optimal adsorption performance.

It is evident from the graph that fluoride removal efficiency increases progressively with contact time for all adsorbents, reaching a maximum at approximately 60 minutes. Beyond this duration, the adsorption rate stabilizes, indicating that equilibrium has been achieved and that most of the available active sites on the adsorbent surface are occupied. [27] The initial rapid increase in fluoride removal can be attributed to the abundance of unoccupied active sites and strong electrostatic attraction between fluoride ions and positively charged alumina surfaces. As adsorption progresses, the remaining sites become less accessible due to repulsive forces between adsorbed and free fluoride ions, leading to a slower rate of adsorption.

Among the three materials, pure activated alumina exhibited slightly higher removal efficiency compared to Ca@AA and Ca-Mg@AA, which maintained moderate but stable adsorption throughout the contact period. The consistent performance of Ca-Mg@AA over time suggests improved structural stability and surface activity imparted by alkaline earth metal modification. Overall, an equilibrium time of **60 minutes** is sufficient for effective fluoride adsorption, beyond which no significant improvement in removal efficiency is observed.

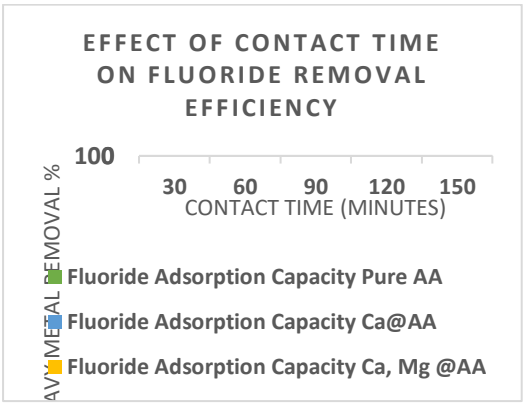

Figure 10: Effect of contact time on Fluoride Removal Efficiency of pure AA, Ca@AA and Ca, Mg@AA

Journal of Chemical Health Risks
www.jchr.org
JCHR (2025) 15(6), 3292-3301 | ISSN:2251-6727

To understand the interaction between the adsorbate and adsorbent surface, the equilibrium data were analyzed using both **Langmuir** and **Freundlich** isotherm models and shown in figure 11.[28] The **Langmuir isotherm** assumes monolayer adsorption on a homogenous surface with identical binding sites and no interaction between adsorbed species. The adsorption parameters presented in Table 2 show the relationship between the initial metal ion concentration (C_i) and the equilibrium concentration (C_e) for evaluating adsorption behavior.

Table 2: Langmuir and Freundlich Isotherm Data for Ca, Mg @AA

C_i	C_e	q_e	C_e/q_e	logC_e	logq_e
10	2.5	5	0.5	0.39794	0.69897
20	5.7	9.533333	0.597902	0.755875	0.979245
40	12.4	18.4	0.673913	1.093422	1.264818
80	36.9	28.73333	1.284223	1.567026	1.458386
160	98.6	40.93333	2.408795	1.993877	1.612077
320	185.6	89.6	2.071429	2.268578	1.952308

As $C_i$increases from 10 to 320 mg/L, the corresponding equilibrium concentration $C_e$also increases, indicating the gradual saturation of available adsorption sites on the adsorbent surface. The calculated adsorption capacity (q_e) rises significantly from 5 to 89.6 mg/g with increasing C_i, suggesting that a higher driving force for mass transfer at elevated concentrations enhances the uptake of metal ions until surface sites become saturated. The parameters $1/C_e$, $\log C_e$, and $\ln C_e$were derived for use in adsorption isotherm models such as Langmuir and Freundlich, while $1/q_e$and $\log q_e$values were obtained to linearize the respective equations for determining adsorption constants. The systematic increase in $\log q_e$with $\log C_e$indicates a favorable adsorption process, confirming that the adsorbent possesses a high affinity for the metal ions at higher concentrations.

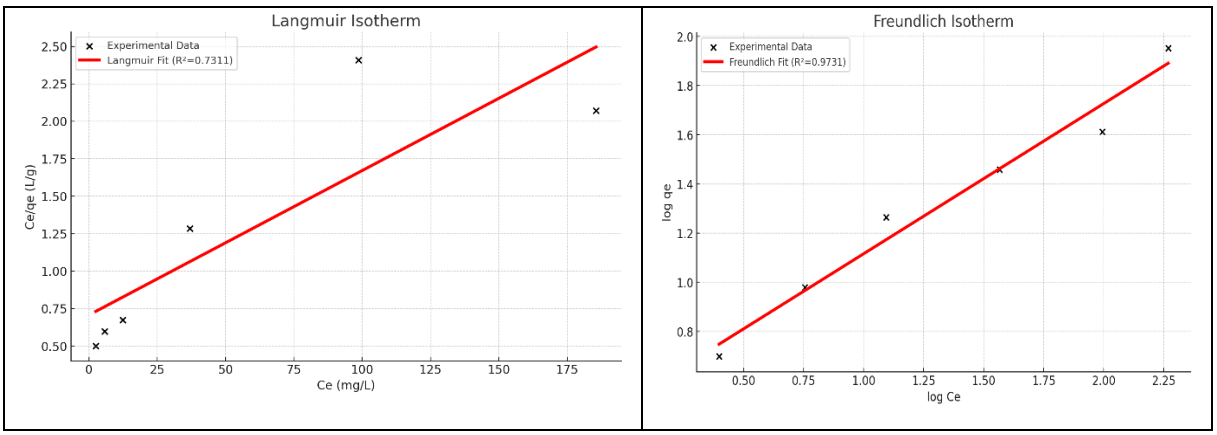

Figure 11: Langmuir and Freundlich isotherm plots for Ca, Mg @AA

The adsorption behavior fits the **Freundlich model** better than the Langmuir model, suggesting that the adsorption mechanism is predominantly heterogeneous and involves interactions beyond simple monolayer coverage.[30]

Conclusions:

Our research effectively validates Ca-Mg-coated activated alumina granules as a superior agent for purging fluoride from groundwater sources. The tailored sol-gel fabrication paired with layered metal deposition produced a nano-porous, crystalline scaffold with enduring coatings, corroborated by detailed material

Journal of Chemical Health Risks

www.jchr.org

JCHR (2025) 15(6), 3292-3301 | ISSN:2251-6727

profiling. Across vital process variables, the upgraded Ca-Mg-AA surpassed standard alumina, securing high fluoride capture in acidic settings and steady results across wider pH levels. Gains in performance arise from amplified reactive surfaces, structural flaws aiding binding, and versatile capture pathways that extend to tackling arsenic and similar toxins. Overcoming drawbacks like pH sensitivity and toxic regenerants in traditional materials, this modification fosters greener, cost-effective purification. Looking ahead, efforts could focus on large-scale trials, gentle reuse methods, and on-site validation in high-risk zones to affirm practicality and longevity. In essence, this advancement offers a viable, enduring strategy to curb fluorosis risks and safeguard potable water for at-risk communities everywhere.

Conflicts of interest:

The author of this manuscript declares no conflict of interest.

Data availability statement:

Data can be available by contacting corresponding author.

References:

1. Shaikh, Mustaq, and Farjana Birajdar. "Groundwater and public health: exploring the connections and challenges." *International Journal for Innovative Science Research Trends and Innovation* 9.2 (2024): 1351-1361.
2. Belekar, R. M., and S. J. Dhoble. "The Fluoride Adsorption Isothermal Studies of Activated Alumina Modified with Different Materials: A Critical Review." *Water Pollution Sources and Purification: Challenges and Scope* (2022): 28-74.
3. Roy Chowdhury, Nilanjana, et al. "A Vivid Picture of the Distribution, Impact, and Consequences of Fluoride in Indian Perspective." *Ground Water Contamination in India: Adverse Effects on Habitats*. Cham: Springer Nature Switzerland, 2024. 83-103.
4. Balali-Mood, Mahdi, et al. "Recent advances in the clinical management of intoxication by five heavy metals: Mercury, lead, chromium, cadmium and arsenic." *Heliyon* 11.4 (2025).
5. Belekar, R. M., and S. J. Dhoble. "Review on Water Purifications Techniques and Challenges." *Water Pollution Sources and Purification: Challenges and Scope*. Bentham Science Publishers, 2022. 1-27.
6. Alhassan, Sikpaam Issaka, et al. "Fluoride removal from water using alumina and aluminum-based composites: A comprehensive review of progress." *Critical Reviews in Environmental Science and Technology* 51.18 (2021): 2051-2085.
7. Fan, Xiaochun, et al. "Improving the chloride binding capacity of alkali activated slag by calcium and aluminum enriched minerals." *Journal of Building Engineering* 70 (2023): 106384.
8. Stoiber, Tasha, et al. "Simultaneous Removal of Co-occurring Contaminants Reduces Drinking Water-Attributed Cancer Risk: A United States Case Study." *Environmental Research* (2025): 122125.
9. Belekar, R. M. "Structural and electrical studies of nanocrystalline Fe2O3 prepared by microwave assisted solution combustion method with mixed fuel approach." Journal of Physical Sciences, Vol. 23, 2018, 189-199
10. Qu, Jiaoyang, et al. "Preparation of CaCO3 coated corundum aggregates by dip-coating and heat treatment and its effects on the properties and microstructures of Al2O3–MgO castables." *Ceramics International* 48.4 (2022): 5174-5186.
11. Wani, Mashooq A., Shubhangi A. Athawale, and R. M. Belekar. "Synthesis, characterization, and exploring optical pathways of centrosymmetric Li2MgP2O7/ZnMgP2O7: Eu3+ pyrophosphate phosphor for LEDs applications." *Journal of Molecular Structure* 1285 (2023): 135466.
12. Kakde, Anand S., et al. "Exploration of Ce+ 3 substitution on electron density distribution, optical, and magnetic properties of Ni-Co-Zn spinel nano-ferrites." *Journal of Sol-Gel Science and Technology* 107.2 (2023): 401-416.
13. Wani, M. A., R. M. Belekar, and B. A. Shingade. "Study of photoluminescence properties of MgAl2O4 doped with europium prepared by microwave assisted solution combustion synthesis." *AIP Conference Proceedings*. Vol. 2104. No. 1. AIP Publishing LLC, 2019.

Journal of Chemical Health Risks

www.jchr.org

JCHR (2025) 15(6), 3292-3301 | ISSN:2251-6727

14. Belekar, R. M., and S. J. Dhoble. "Activated Alumina Granules with nanoscale porosity for water defluoridation." *Nano-Structures & Nano-Objects* 16 (2018): 322-328.
15. Wani, M. A., et al. "Energy transfer mechanism of Eu2+, Mn2+ Doped lithium aluminate phosphor: Synthesis, Hirshfeld surface analysis and optical study." *Materials Chemistry and Physics* 292 (2022): 126796.
16. Sanni, Abdulkadeem, et al. "Unveiling a paradigm shift in supercapacitor dynamics: γ-Al2O3-infused ZnO nanorods with redox-active K4Fe (CN) 6 alkaline electrolytes." *Journal of Alloys and Compounds* 1010 (2025): 177892.
17. Liu, Yan, et al. "Valence engineering via selective atomic substitution on tetrahedral sites in spinel oxide for highly enhanced oxygen evolution catalysis." *Journal of the American Chemical Society* 141.20 (2019): 8136-8145.
18. Baraton, M. I., P. Quintard, and P. Chagnon. "Infrared determination of α-alumina in plasma sprayed λ-alumina." *Materials chemistry and physics* 10.5 (1984): 413-424.
19. Saadati, Masoud, and Salva Sadigzadeh. "Surface-Modified γ-Alumina Nanoparticles for Efficient Adsorption of some Cationic Dyes from Wastewater." *ecosystems* 1 (2025): 2.
20. Puchakayla, Pranith Kumar Reddy, et al. "Defects evolution during printing, debinding and sintering for additive manufacturing of yttria stabilized zirconia." *Materials Characterization* 221 (2025): 114752.
21. Koehler, A., et al. "Phase and porosity changes in a calcium aluminate cement and alumina system under hydrothermal conditions." *Ceramics International* 49.3 (2023): 4659-4667.
22. Li, Cong, et al. "Analysis of internal energy and mass loss rate of fuel with water sublayer at different initial temperatures." *Energy* 283 (2023): 129037.
23. El Hosry, Leina, et al. "Sample preparation and analytical techniques in the determination of trace elements in food: A review." *Foods* 12.4 (2023): 895.
24. Chen, Yingxin, et al. "Adsorption of fluoride from aqueous solutions using graphene oxide composite materials at a neutral pH." *Journal of Molecular Liquids* 377 (2023): 121467.
25. Jiang, Guomin, et al. "Structural modification of aluminum oxides for removing fluoride in water: crystal forms and metal ion doping." *Environmental Technology* 43.21 (2022): 3248-3261.
26. Wang, Lanyang, et al. "Enhancement of carbon dioxide adsorption performance on mesoporous alumina modified with alkaline earth metals." *Colloids and Surfaces A: Physicochemical and Engineering Aspects* 690 (2024): 133823.
27. Murphy, Orla P., et al. "A review on the adsorption isotherms and design calculations for the optimization of adsorbent mass and contact time." *ACS omega* 8.20 (2023): 17407-17430.
28. Pereira, Sharon K., et al. "A simplified modeling procedure for adsorption at varying pH conditions using the modified Langmuir–Freundlich isotherm." *Applied Water Science* 13.1 (2023): 29.
29. Alafnan, Saad, et al. "Langmuir adsorption isotherm in unconventional resources: Applicability and limitations." *Journal of Petroleum Science and Engineering* 207 (2021): 109172.
30. Shimizu, Seishi, and Nobuyuki Matubayasi. "Understanding sorption mechanisms directly from isotherms." *Langmuir* 39.17 (2023): 6113-6125.